Surface Enhanced Raman Spectroscopy and Theoretical Studies on 1,4-Dihydrazinophthalazine Sulfate†

I. Pavel,‡ D. Moigno,‡ S. Cîntă,§ and W. Kiefer*,‡

Institut für Physikalische Chemie der Universität Würzburg, Am Hubland, D-97074 Würzburg, Germany, and Physics Department, Babeş-Bolyai University, Kogălniceanu 1, RO-3400 Cluj-Napoca, Romania

Received: May 17, 2001; In Final Form: October 30, 2001

The two tautomeric forms of 1,4-dihydrazinophthalazine sulfate have been studied by means of density functional theory calculations. The computed structural parameters agree very well with the experimental values of the related crystal structure. The SERS spectrum of 1,4-dihydrazinophthalazine sulfate was then recorded at different solution concentrations and discussed on the basis of the SERS "surface selection rules" in conjunction with the results of theoretical calculations. 1,4-Dihydrazinophthalazine sulfate was found to be mainly chemisorbed on the Ag colloid and to not undergo photochemistry to a photoproduct as reflected by the SERS spectra and calculations. At about 10^{-6} mol L^{-1} the molecular skeletal plane is probably oriented perpendicular to, or at least significantly tilted with respect to, the Ag surface plane. With the increase in solution concentration, a surface coverage with 1,4-dihydrazinophthalazine sulfate may occur.

Introduction

1,4-Dihydrazinophthalazine (DHPZ) sulfate possesses a wide range of applications from the well-known antihypertensive agent[1,2] to the available pharmaceutical analytical reagent.[3] DHPZ was involved in the synthesis of some copper[4,5] and lead[6] complexes and new biologically active compounds[7−9] characterized by ESR, NMR, or IR spectroscopy. Efforts have been directed toward studying the influence of these DHPZ drugs on arterial pressure, cardiac rate, and urinary excretion of catecholamines at low concentrations.[9−11]

Raman spectroscopy is a useful tool for recording fingerprints of molecules.[12−14] However, owing to its low scattering cross-section, and the possibility of high background-fluorescence interference, the application of Raman spectroscopy to trace analysis is limited. Although the theories explaining SERS are not definite and still evolving, the experimental research and development in recent years has demonstrated SERS to be a potential technique for environmental and biological trace analysis, enabling the detection of even single molecules.[15] Moreover, SERS spectroscopy can provide information about the changes of molecular identity or orientation to the metal surface with the concentration.[16,17] Therefore, Raman and SERS spectra of DHPZ sulfate were recorded for the first time at different concentrations and discussed with the assistance of results obtained from density functional theory (DFT) calculations. Here it is taking into account that these theoretical methods can efficiently and accurately predict the electronic and structural properties, as well as vibrational modes, of biologically important systems.[18,19] Its vibrational behavior at low concentrations was closely examined to determine a possible unwanted surface photochemistry. A Ag colloid served as an artificial biological interface in this case.

Several studies[20,21] have shown the acidic atoms of DHPZ derivatives to be quite mobile, allowing tautomeric equilibrium in solution. Protonation is usually formulated at the two terminal amino groups **1** (Figure 1). Obviously, this is in keeping with an assumed substituted hydrazine character of the base. For the alternative tautomeric form **2** (Figure 1), one proton is bonded to the phthalazine N2 and the other to the hydrazino N4. Therefore, to establish and characterize the tautomeric forms, the structures of those were calculated and optimized with density functional methods at different levels of theory.

Experimental Section

Sample and Instrumentation. All starting materials involved in substrate and solutions preparation were purchased from commercial sources as analytically pure reagents.

The FT-Raman measurement of DHPZ sulfate solid powder was performed using a Bruker IFS 120-HR spectrometer with an integrated FRA 106 Raman module. Radiation of 1064 nm from a Nd:YAG laser was employed for excitation. A Ge detector was used and cooling was with liquid nitrogen. The spectral data were analyzed using OPUS 2.0.5 software. The SERS spectra of DHPZ sulfate on Ag colloid in the visible wavelength region were recorded with a Spex 1404 double spectrometer with 2400 grooves/cm gratings. The 514.5 nm output of a Spectra Physics argon ion laser was used as the excitation line. The backscattering geometry was adopted to collect the SERS spectra. The laser excitation was coupled to an optical microscope Olympus U-CMAD-2 with two objectives: DPLAN 20 160/0.17 and ULWD MS-PLAN 80/0.75. Noteworthy features of this instrumentation are a notch filter to reject Rayleigh scattering and a liquid nitrogen-cooled charge-coupled device (Photometrics model 9000 CCD camera) to provide state-of-the-art quantum efficiency in Raman detection. The MAPS VO 98.5 analyzing software package was used in this case for the acquisition of data. In both cases the spectral resolution was 2 cm^{-1} and the output laser power 500 mW.

† Part of the special issue "Mitsuo Tasumi Festschrift".

* Corresponding author. E-mail: wolfgang.kiefer@mail.uni-wuerzburg.de. Fax: +49 (0)931 888 6332.

‡ Universität Würzburg.

§ Babeş-Bolyai University.

10.1021/jp011910l CCC: $22.00
Published on Web 01/04/2002

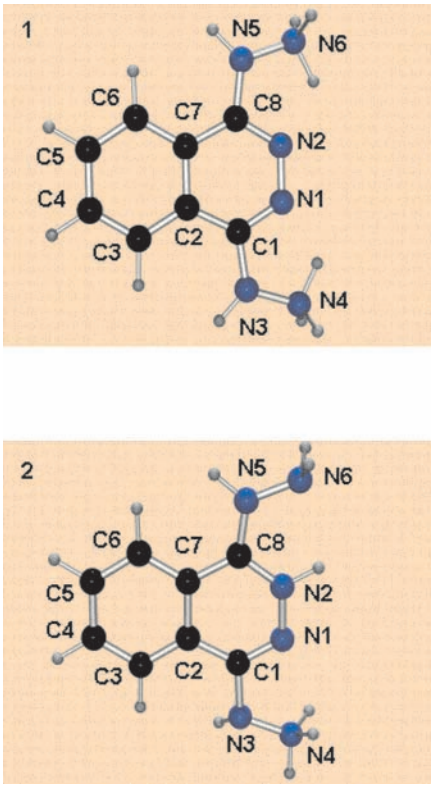

Figure 1. B3LYP/6-311+G(d) optimized geometry of DHPZ sulfate tautomers **1** and **2**.

A sodium-citrate-reduced Ag colloid was employed as SERS substrate. Ag colloid was prepared according to the literature.[23] Small amounts of DHPZ sulfate 10^{-3} M water solutions were added to 0.7 mL of colloid. NaCl solution (10^{-2} M) was also added (10:1) to produce a stabilization of the colloidal dispersion and a considerable enhancement of the SERS spectrum.[24] Final concentrations of sample were 6.9×10^{-7}, 1.4×10^{-6}, 4.2×10^{-6}, 4.0×10^{-5}, and 1.2×10^{-4} mol L^{-1}.

Computational Details

The DFT calculations were performed using Gaussian 98.[25] Becke's 1988 exchange functional[26] in combination with the Perdew-Wang 91 gradient-corrected correlation functional (BPW91),[27] and Becke's three-parameter hybrid exchange functional[28,29] using the LYP correlational functional of Lee, Yang, and Parr (B3LYP)[30] were employed in calculations. The 6-31+G(d) and 6-311+G(d) Pople split valence basis sets were chosen in the geometry optimization and the normal modes calculations, taking into account that results obtained with a split valence set are a significant improvement on those obtained with a minimal basis set.[31] In the case of tautomeric form **1**, these calculations were performed with C_2, C_s, and C_{2v} restricted symmetries. By adding polarization and diffuse functions to the split valence set, the calculated structural parameters and vibrational modes are more accurate. DFT calculations on harmonic vibrational modes were performed by using fully optimized molecular geometry, and the analytical harmonic vibrational wavenumbers for all structures confirmed that local minima on the potential energy surface have been found.

Results and Discussion

Geometry Optimization. The optimized structures of DHPZ sulfate tautomeric forms, which have been computed at high levels of theory using the B3LYP/6-311+G(d) method, are presented in Figure 1. Protonation is at the two terminal amino groups in **1** or at the N2 and N4 atoms in **2**. The structural parameters of **1** and **2**, calculated with BPW91/6-31+G(d), 6-311+G(d), and B3LYP/6-31+G(d), 6-311+G(d) methods are listed in Table 1. To assess the accuracy of the geometry optimizations, the computed structural parameters for tautomer **2** were compared to experimental values of the related crystal structure. The calculated bond distances and bond angles of tautomer **2** are very close to the reported parameters.[21] To the best of our knowledge, no crystal structure data for the tautomeric form **1** were yet published. The two theoretical methods agree quite well with each other, but the bond lengths and angles of **2** were better reproduced in almost all cases by the B3LYP/6-311+G(d) method, where the maximum discrepancy was only 3 pm and 2.5° with respect to the experimental data.[21] Also, the agreement between computed and experimental values improved, but not very significantly, from the 6-31+G(d) to 6-311+G(d) level of theory.

On the basis of the geometry optimizations that have been carried out, the following conclusions can be reached. The phthalazine unit is almost planar in both diprotonated forms **1** and **2**. The fragment C2−C3−C4−C5−C6−C7 is planar and the deviations of the other atoms from this plane are similar in the two forms. The pyridazine rings deviate slightly from planarity, adopting distorted boat conformations with the N2 and C2 atoms out of the plane.[21,22,32,33] The calculated angle between the best planes through the benzene ring and the pyridazine is 1.45° and 1.36° for the tautomer **1** and **2**, respectively, with the best basis set 6-311+G(d) and the B3LYP functional. The method BPW91/6-311+G(d) led to a value of 1.42° and 1.02° for **1** and **2**, respectively, also comparable to the literature value of 1.59° for tautomer **2**.[21] The $-NH-NH_2$ substitute at C8 is in the plane of the ring and the experimental and calculated (Table 1) values for the N5−C8 interatomic distance indicate a partially double bond with the phthalazine unit. Indeed, the N2−C8−N5−N6 dihedral angle calculated for **2** with the B3LYP/6-311+G(d) and BPW91/6-311+G(d) methods is 0°, as expected. In the case of the $-NH-NH_3^+$ substitute at C1, the bonds at N3 are not planar and a much weaker conjugation with the phthalazine system can be inferred. This should lead to a higher value for the N1−C1−N3−N4 dihedral angle of **2**. The B3LYP/6-311+G(d) and BPW91/6-311+G(d) methods predicted an absolute value of 3.2° and 3.6°, which confirmed these aspects. For the tautomer **1**, these methods predicted an absolute value of 8.3° and 8.5°, respectively, which suggests a much weaker conjugation with the phthalazine system.

The positive charge resulting from the protonation of N2 is delocalized over the N2−C8−N5 fragment. The structure of **2** should therefore be represented in solution by a mesomeric equilibrium between the limiting formulas **2a** and **2b** (Figure 2). With the B3LYP/6-311+G(d) method, the N2−C8 bond is 4.5 pm longer than N1−C1 and N5−C8 is 8.5 pm shorter than N3−C1. The comparison of the same bond lengths, calculated with the BPW91/6-311+G(d), yields a similar difference of 4.5 and 7.8 pm, respectively, owing to the charge delocalization over the N2−C8−N5 moiety. Due to the protonation at the two terminal amino groups in tautomer **1**, the N2−C8 and N1−C1 bond lengths have identical values of 131.6 and 130.2 pm, respectively, with the BPW91/6-311+G(d) and B3LYP/6-311+G(d) methods. For N5−C8 and N3−C1, the BPW91/6-311+G(d) and B3LYP/6-311+G(d) methods predict bond lengths of 142.1 and 142.0 pm.

The absolute energy difference ΔE_0 between **1** and **2**, which contains the zero-point energy (ZPE) correction, has been

TABLE 1: Selected Structural Parameters Calculated for the DHPZ Sulfate Tautomers 1 and 2, Respectively, Together with the Experimental Values Found in Tautomeric Form 1

		calc for **2**				calc for **1**			
		BPW91		B3LYP		BPW91		B3LYP	
	exp in **2**[22]	6-31+G(d)	6-311+G(d)	6-31+G(d)	6-311+G(d)	6-31+G(d)	6-311+G(d)	6-31+G(d)	6-311+G(d)
					Bond Lengths (pm)				
N1−C1	129.6(5)	131.0	130.5	129.6	129.6	132.1	131.6	130.7	130.2
N2−C8	131.3(5)	135.4	135.0	134.4	134.1	132.1	131.6	130.7	130.2
N3−N4	141.5(5)	144.3	144.1	143.7	143.6	144.3	144.1	143.7	143.5
N5−N6	141.5(5)	140.9	140.7	140.6	140.4	144.3	144.1	143.7	143.5
N3−C1	141.0(5)	142.7	142.3	142.1	142.1	142.2	142.1	142.0	142.0
N5−C8	134.0(5)	134.7	134.5	133.9	133.6	142.3	142.1	142.0	142.0
N1−N2	137.9(4)	135.4	135.1	135.4	135.2	135.1	134.9	135.2	135.0
C1−C2	142.1(5)	144.7	144.4	144.6	144.4	143.7	143.5	143.5	143.3
C7−C8	144.8(5)	145.1	145.0	144.9	144.7	143.7	143.5	143.5	143.3
C2−C3	140.7(5)	141.3	141.0	140.6	140.3	141.6	141.2	141.0	140.7
C6−C7	138.1(5)	141.2	141.0	140.6	140.4	141.6	141.2	141.0	140.7
C2−C7	141.8(5)	143.6	143.3	142.6	142.4	143.9	143.5	142.8	142.5
C4−C5	140.8(6)	141.1	140.7	140.5	140.2	141.5	141.2	141.0	140.7
C3−C4	135.7(6)	139.0	139.3	139.0	138.7	139.4	139.0	138.7	138.3
C5−C6	138.0(6)	139.2	139.2	139.0	138.6	139.4	139.0	138.7	138.3

		calc for **2**				calc for **1**			
		BPW91		B3LYP		BPW91		B3LYP	
	exp in **2**[22]	6-31+G(d)	6-311+G(d)	6-31+G(d)	6-311+G(d)	6-31+G(d)	6-311+G(d)	6-31+G(d)	6-311+G(d)
					Angles (deg)				
C1−C2−C3	124.3(3)	124.0	124.0	123.8	123.9	125.0	125.0	125.0	125.0
C6−C7−C8	123.9(3)	123.3	123.2	123.2	123.2	125.0	125.0	125.0	125.0
C1−C2−C7	117.4(3)	116.4	116.4	116.5	116.5	115.4	115.4	115.4	115.3
C2−C7−C8	116.1(3)	117.3	117.5	117.3	117.3	115.4	115.4	115.4	115.3
C3−C2−C7	118.3(3)	119.6	119.3	119.6	119.6	119.6	119.6	119.6	119.6
C2−C7−C6	120.1(3)	119.4	119.5	119.5	119.4	119.6	119.6	119.6	119.6
C2−C3−C4	120.9(4)	120.0	120.1	120.0	120.0	119.8	119.8	119.7	119.7
C5−C6−C7	120.7(4)	120.1	120.2	120.0	120.1	119.8	119.8	119.7	119.7
C3−C4−C5	120.5(4)	120.4	120.4	120.5	120.5	120.6	120.6	120.6	120.6
C4−C5−C6	120.5(4)	120.5	120.5	120.5	120.5	120.6	120.6	120.6	120.6
N2−C8−N5	118.1(3)	116.8	116.8	117.4	117.4	114.0	114.0	114.7	114.7
N1−C1−N3	115.0(3)	115.4	115.0	115.6	115.6	114.0	114.0	114.7	114.7
N2−C8−C7	119.8(3)	118.2	118.2	118.1	118.1	124.5	124.5	124.6	124.6
N1−C1−C2	125.4(3)	125.0	124.4	124.8	124.8	124.5	124.5	124.6	124.6
N5−C8−C7	122.1(3)	125.0	125.0	124.5	124.5	121.4	121.4	120.6	120.6
N3−C1−C2	119.5(3)	119.6	120.0	119.5	119.5	121.4	121.4	120.6	120.6
N2−N1−C1	116.0(3)	116.7	116.7	117.1	117.2	120.0	120.0	120.0	120.0
N1−N2−C8	125.2(3)	126.3	125.7	126.0	125.9	120.0	120.0	120.0	120.0
N4−N3−C1	112.6(3)	112.8	112.7	113.1	113.0	111.3	111.3	112.1	112.1
N6−N5−C8	116.6(3)	118.2	118.1	118.5	118.4	111.3	111.3	112.1	112.1

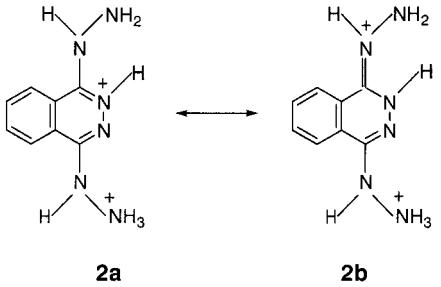

Figure 2. Depiction of the mesomeric equilibrium of **2**.

determined to be 42.7 and 48.5 kJ/mol with the BPW91/6-31+G(d) and 6-311+G(d) methods. With the B3LYP/6-31+G(d) and 6-311+G(d) methods, ΔE_0 has been predicted to be 63.7 and 54.9 kJ/mol, respectively. Therefore, according to our DFT calculations results, the tautomeric form **1** is thermodynamically the most favorized one.

After the geometry optimization of **1** with a C_2, C_s, and C_{2v} restricted symmetry (BPW91/6-311+G(d) method), the absolute energy difference between these imposed structures of **1** has been also determined. Either with C_2 symmetry or C_s symmetry, the absolute energy difference with respect to C_{2v} has been found to be 12.6 kJ/mol (Figure 3). This seems to indicate the structure of C_2 or C_s symmetry as the most stable one, due probably to the fact that, in those cases, resonance interaction between the nitrogen lone-pair orbital and the ring is possible. As depicted in Figure 3, in the case of C_{2v} symmetry, the three groups around N are coplanar, with sp^2 hybridization, and the axis of symmetry of the lone-pair orbital

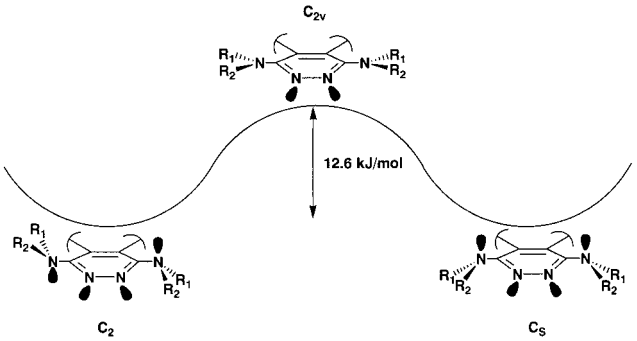

Figure 3. Calculated possible geometry of tautomeric form **1** of different symmetries.

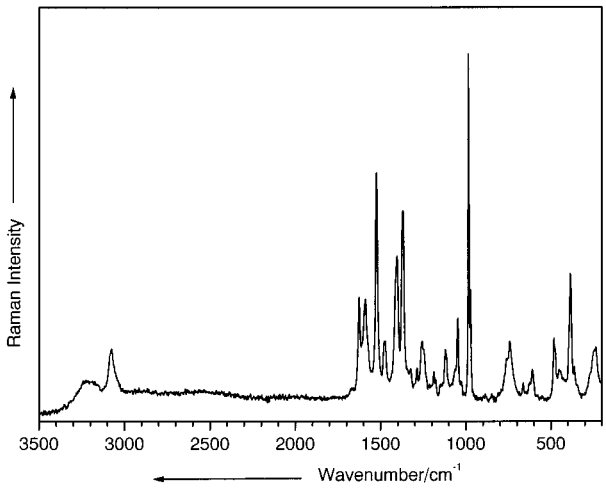

Figure 4. FT-Raman spectrum of DHPZ sulfate solid powder. Excitation line: 1064 nm.

is in the plane of the ring corresponding to no overlap and complete elimination of conjugation.

Vibrational Spectroscopy. The FT-Raman spectrum of DHPZ sulfate recorded in the 200−3500 cm^{-1} spectral region is presented in Figure 4. The observed bands as well as the vibrational assignment are summarized in Table 2. In a number of instances, theoretical calculations have aided the interpretation of Raman spectra and many previous incomplete or incorrect assignments have been analyzed and improved. Moreover, for a correct interpretation of the SERS data, it is necessary to have a complete vibrational assignment of the DHPZ sulfate FT-Raman spectrum as a guideline. Consequently, the vibrational fundamentals from the Raman spectrum were analyzed by comparing the vibrational modes with those assigned for phthalazine[17,34,35] and naphthalene[36,37] in conjunction with theoretical calculations. Ab initio harmonic vibrational wavenumbers (ω) are typically larger than the fundamentals (ν) experimentally observed.[38] The vibrational assignment in the experimental spectrum was feasible with the help of the BPW91 calculations (Table 2), as expected. Consistent with previous findings,[39,40] the B3LYP functional tends to overestimate fundamental modes. Indeed, the calculated vibrational wavenumbers using B3LYP are much larger than those using BPW91 compared to the experimental fundamentals and should be scaled in order to be in good agreement with the experiment.[41] Major sources of this disagreement are the neglect of anharmonicity effects in the theoretical treatment and the incomplete incorporation of electron correlation. We wish to remark that vibrational modes calculated with the 6-311+G(d) basis set improved, but not significantly, the calculated values.

The observed bands in the SERS spectrum of DHPZ sulfate (Figure 4) were also given in Table 2 after the complete analysis of the FT-Raman spectrum.

It is well-known that there are two possibilities of molecules adsorption on the metal surface, namely physisorption and chemisorption. In the case of physisorption, the molecules have a SERS spectrum similar to that of the free molecules, due to a relatively larger distance between metal surface and adsorbed compound. Comparatively, in the case of chemisorption there is an overlapping of the molecular and metal orbitals, the molecular structure being changed, and consequently, the position of the bands and their relative intensities are dramatically changed.

Comparing the FT-Raman and SERS spectra of DHPZ sulfate (6.9×10^{-7} mol L^{-1}) (Figure 5) on Ag sol, one may notice that there are major differences between the band positions and their relative intensities. Therefore, we suppose that DHPZ sulfate is mainly chemisorbed on the silver surface. According to the adatom model proposed by Otto et al.,[42,43] chemisorption occurs in specific active sites of the metal surface and the SERS signal is mainly generated by a minority species formed at these surface sites. Indeed, all of the prominent lines (1452, 1382, 1019, 799, and 529 cm^{-1}) of the SERS spectrum are assignable to totally symmetric modes of phthalazine and the overall spectral feature has a striking resemblance to the SERS spectrum of phthalazine. That indicates a strong interaction of the molecule through the phthalazine part with the silver surface. Moreover, the NH_3^+ asymmetric bending and torsion modes, which were attributed at 1628 and 268 cm^{-1}, respectively, in the FT-Raman spectrum of DHPZ sulfate and do not overlap with another vibrational modes, are absent or very weak in the SERS spectrum. Also, the NH bending, N−N stretching, and SO_4^{2-} stretching or bending modes, which were assigned at 1477, 1122, 1063, and 475 cm^{-1}, respectively, in the FT-Raman spectrum, have a similar behavior. Therefore, the terminal parts may be far from the surface. Strong evidence for decreasing SERS intensity or absence of some vibrational modes, when a vibrational group is separated several ångstroms from the surface, has been found in other studies too.[44]

Recently, the SERS spectrum of phthalazine adsorbed on silver colloid was reexamined on the basis of results obtained in a flow cell and the conclusion[17,45] was drawn that many of the spectroscopic changes attributed to various factors, such as excitation wavelength, concentration, and coadsorption of anions, were, in fact, due to the surface photodecomposition of phthalazine. Its photoreaction was ascribed to a process in which the N−N bond of the molecule breaks to form an adsorbed species (with the newly free N ends forming two Ag−N bonds) resembling an ortho-disubstituted benzene. The suggested structure of the photoproduct implies that the vibrational signature of the benzene ring should dominate the SERS spectrum. Although the SERS spectrum of DHPZ sulfate was recorded again with a longer exposure time (100, 200, and 250 s), the rapidly growing bands of ortho-substituted benzenes, which were observed in the SERS spectrum of phthalazine[17,45] on Ag colloid with the same excitation line, were either absent or very weak. Namely, the signals at 1547, 1465, 1432, 1332, 1278, and 545 cm^{-1}, respectively, due to the ν8a, 19b, 19a, 14, 3, and 6a vibrational modes of ortho-substituted benzenes[46] were absent, whereas the observed bands at 1244, 755, and 483 cm^{-1}, respectively, assigned to the ν7a, 11, and 6b vibrational modes of the same species were very weak and did not dominate the SERS spectrum of DHPZ sulfate. Therefore, we suggest that there are no photoproducts from a photoreaction of DHPZ sulfate at this concentration (6.9×10^{-7} mol L^{-1}) and the mentioned bands can be indeed assigned to the native adsorbate.

The highest occupied molecular orbital (HOMO), the lowest unoccupied molecular orbital (LUMO), and LUMO+1 are shown in Figure 6. Since the LUMO and LUMO+1 are energetically very close (9.56 and 9.40 eV), both of them should be taken into consideration when one analyzes the possible appearance of photoproducts during the irradiation of the adsorbate. The LUMO, which is partially situated at the N1−N2 atoms has a bonding character, whereas at the N2−C8 and N1−C1 atoms it has an antibonding one. A closer examination of the LUMO+1 shows a reverse behavior at the mentioned atoms. Populating these orbitals during the irradiation should lead in the first case (LUMO) to a breaking of the C1−N1 and C8−N2 bonds, followed by an N_2 emission, and in the second

TABLE 2: Selected Calculated and Experimental Raman and SERS Data (cm^{-1}), Together with Their Tentative Assignment

	calc					
	BPW91		B3LYP		SERS 6.9 ×	
Raman	6-31+G(d)	6-311+G(d)	6-31+G(d)	6-311+G(d)	10^{-7} mol L^{-1}	vibrational assignment
1628 (m)	1622	1624	1674	1767		NH_3^+ asym bending
1591 (m)	1601	1596	1647	1641	1606 (m)	ring stretching + NH bending + CH bending
1570 (sh)	1573	1568	1625	1618	1577 (m)	NH_3^+ sym bending + ring stretching
1525 (s)	1521	1519	1565	1571	1531 (m)	CH bending + NH bending + NH_3+ asym bending
					1491 (w)	ring stretching + CH bending
1477 (w)	1488	1483	1537	1523		NH bending + NH_3^+ asym bending
1404 (m)	1416	1412	1463	1457	1452 (vs)	ring stretching + CH bending
1370 (ms)	1379	1370	1401	1395	1382 (vs)	ring stretching
	1363	1358	1387	1375	1360 (m)	ring stretching + CH bending
1323 (vw)	1336	1335	1377	1373	1313 (w)	ring stretching + NH bending
1286 (vw)	1274	1276	1314	1313		CH bending + NH_3^+ sym bending
1258 (w)	1229	1233	1253	1250	1240 (sh)	CH bending + ring stretching + C−N stretching
1248 (w)	1194	1194	1220	1222	1229 (w)	+ NH bending + NH_3^+ rocking
1189 (vw)	1189	1187	1219	1217		CH bending + NH_3^+ rocking
1177 (vw)	1177	1177	1207	1207	1161 (w)	CH bending
1122 (vw)						SO_4^{2-} asym stretching
1115 (vw)	1091	1096	1126	1122	1116 (vw)	skeletal distortion
1063 (sh)	1074	1076	1110	1108		SO_4^{2-} sym stretching + skeletal distortion + N−N stretching
1048 (w)	1037	1040	1064	1060	1061 (vw)	CH bending + ring stretching
1029 (vw)	1014	1015	1042	1042		N−N stretching + CH bending
986 (vs)	997	1001	1024	1021	1019 (s)	ring breathing
974 (m)	999	994	988	984	988 (m)	CH wagging
					943 (w)	skeletal distortion
	951	946	887	882	924 (vw)	CH wagging
762 (sh)	760	764	790	787	799 (ms)	ring stretching + CH wagging
744 (w)	750	748	766	766	755 (vw)	skeletal torsion
663 (vw)	651	651	678	676	668 (vw)	skeletal distortion + CH wagging
	648	648	672	674	653 (vw)	
624 (sh)	630	629	648	649	623 (vw)	skeletal distortion + NH_3^+ rocking
611 (vw)					607 (vw)	SO_4^{2-} asym bending
					529 (m)	skeletal distortion
					519 (vw)	skeletal distortion
483 (w)	472	473	486	486	483 (vw)	skeletal torsion
475 (vw)	465	466	479	479		SO_4^{2-} sym bending + NH bending + skeletal bending
386 (m)	392	389	401	406		NH_3^+ bending + NH bending + skeletal distortion
362 (vw)	372	369	377	378		NH_3^+ bending + NH bending + skeletal distortion
268 (sh)	288	288	240	240		NH_3^+ torsion
235 (vw)	223	224	214	216	228 (m)	skeletal distortion + Ag−N stretching

[a] Abbreviations: vw, very weak; w, weak; m, medium; ms, medium strong; s, strong; vs, very strong; sh, shoulder.

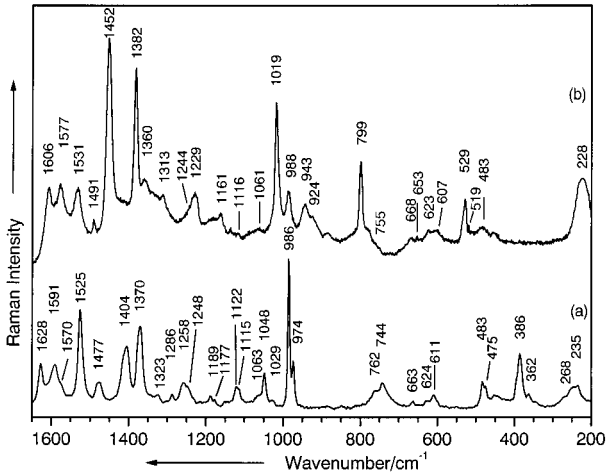

Figure 5. FT-Raman spectrum of DHPZ sulfate solid powder (a) and SERS (b) (6.9×10^{-7} mol L^{-1}) spectrum on Ag colloid. Excitation line: (a) 1064 nm and (b) 514.5 nm.

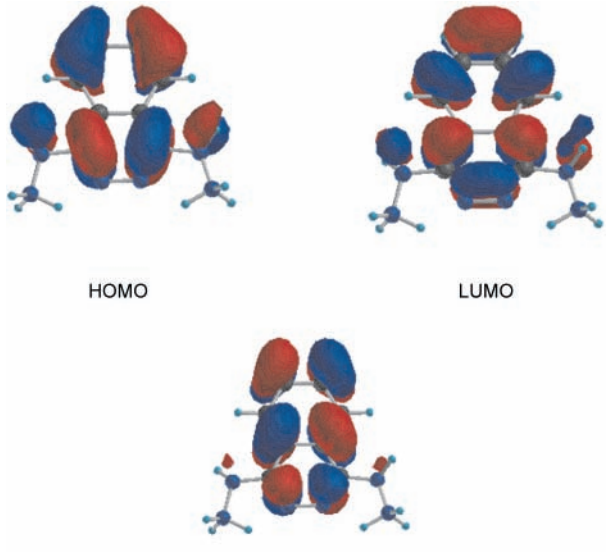

Figure 6. Calculated HOMO, LUMO, and LUMO+1 of DHPZ sulfate with BPW91/6-311+G(d). (Isocontour: 0.03 au)

case (LUMO+1) to a breaking of the N1−N2 bond, as in the model proposed by Suh et al.[17] But, the HOMO−LUMO and HOMO−LUMO+1 gaps of DHPZ sulfate were calculated to be 3.46 and 3.61 eV, which correspond to an absorption in the UV spectral region, namely at 358 and 343 nm, respectively. This could explain the absence of the photoproducts after the excitation of the sample with 514.5 nm, taking into account that the photoreaction reported on phthalazine is only a one-

photon process.[17] However, one should take into consideration that the calculations refer to the gas phase and do not describe the interaction of the molecule with the Ag surface.

It is well-known that the determination of orientation of molecules adsorbed on metal surfaces is based on SERS "surface selection rules".[47,48] These stated that vibrations deriving their intensities from a large value of α_{zz} (with *z* lying to the local metal surface normal) would be the most intense in the SERS spectrum when the molecule has an end-on orientation to the Ag surface. According to the mentioned rules, we have tried to establish the orientation of DHPZ sulfate on the Ag colloid, at different concentration.

Figure 6 shows the SERS spectrum of DHPZ sulfate at different concentrations. Examining the SERS spectra of DHPZ sulfate recorded at 6.9×10^{-7}, 1.4×10^{-6}, and 4.2×10^{-6} mol L^{-1} (Figure 6a−c, respectively), one can notice again that all of the strong bands (1452, 1382, 1019, 799, and 529 cm^{-1}, respectively, in the SERS spectrum (a)) are in-plane totally symmetric modes of phthalazine. In all these spectra, the mentioned bands are very little shifted in comparison to those of the SERS spectrum at lowest concentration (a) (Figure 6). The bands at 1452 (very strong), 1382 (very strong), and 799 cm^{-1} (medium to strong) are good candidates for modes with a much higher α_{zz} term than the other Raman polarizability components, since they are in-plane (of the molecule) ring stretching vibrations. Moreover, according to our theoretical calculations, the bands at 1452 and 1382 cm^{-1} are due to in-plane ring stretching modes, which involve stronger C−N, N−N, and C−C bonds, due to the bond delocalization. In the SERS spectrum, the strong band at 1019 cm^{-1} is due to the skeletal breathing, while the medium signal at 529 cm^{-1} is attributed to a skeletal distortion. All of these strong bands correspond according to the literature to a_g modes of naphthalene. This makes them also good candidates for enhancement.[47,48] All those may support the idea that DHPZ sulfate is adsorbed such that the skeletal plane is oriented perpendicular to, or significantly tilted with respect to, the surface. Considering the steric hindrance that could occur at the approaching of the tautomeric form **2** to the surface, we suppose that the interaction of the tautomeric form **1** with the Ag surface is favorized.

Also, the relative magnitude of the intensity of CH stretching bands can play a very important role in analyzing the surface geometry of compounds that have a planar structure.[47,48] In the case of naphthalene, for example, the CH stretching vibrations contribute significantly only to the α_{xy}, α_{xx}, and α_{yy} Raman polarizability components (where *z* is normal to the surface), when the molecule is lying down flat on the surface. If, on the other hand, it is standing up on the surface, the CH stretching vibrations would obtain their intensities from α_{zz}, α_{xz}, and α_{yz}, resulting in a higher SERS intensity for those bands.[47,48] Taking into account that the studied molecule has a strong interaction through the phthalazine part with the Ag surface and that DFT calculations led to an almost planar phthalazine system in both diprotonated forms **1** and **2**, the observation of strong or weak CH stretching bands in the SERS spectrum of DHPZ sulfate would constitute a simple rule for determining the surface geometry of molecule adsorbed on the Ag colloid surface at different concentrations.

The SERS spectrum of DHPZ sulfate at 4.2×10^{-6} mol L^{-1} (Figure 7c) shows a weak to medium broad CH stretching band at 3080 cm^{-1}, not strong, as expected according to the simple rule discussed. This case is similar to that of phthalazine,[48] where the CH stretching bands are very weak even though the molecule stands up on the surface. This is probably due to the fact that

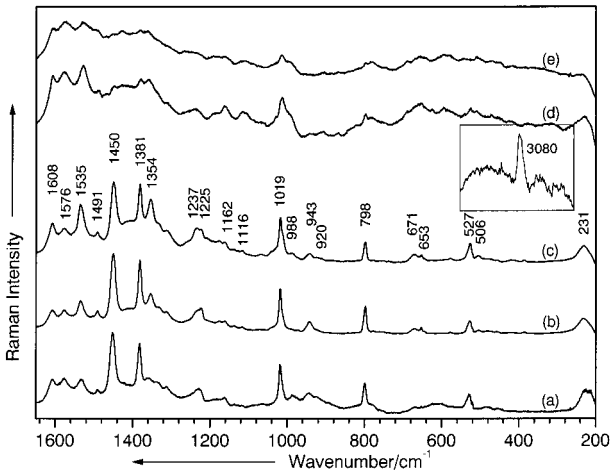

Figure 7. SERS spectra of DHPZ sulfate on Ag colloid at different concentrations: 6.9×10^{-7} mol L^{-1} (a), 1.4×10^{-6} mol L^{-1} (b), 4.2×10^{-6} mol L^{-1} (c), 4.0×10^{-5} mol L^{-1} (d), and 1.2×10^{-4} mol L^{-1} (e). Excitation line: 514.5 nm.

the two CH bonds nearest the surface are parallel to the surface even when the molecule is standing and hence do not contribute greatly to the SERS intensity.[48] However, the signal is stronger than in case of phthalazine, suggesting that the top two CH bonds are closer and rather tilted to the surface than in the case of phthalazine. Therefore, the DHPZ sulfate prefers probably in this case a significantly tilted orientation to the metal surface. The SERS spectrum of DHPZ sulfate at 4.2×10^{-6} mol L^{-1} (c) is different from those at lower concentration (6.9×10^{-7} mol L^{-1} (a)) but not dramatically (Figure 7). It is evident that relative intensities of the Raman lines change with a decrease in the DHPZ sulfate solution concentration. As the concentration is decreased, the band intensity of the CH stretching mode decreases. The molecule tends probably to lie flat on the Ag surface, but the flat orientation is not achieved even at the lowest concentration, since the ring breathing should be at least 10 cm^{-1} shifted along with substantial band broadening in the SERS spectrum (Figure 7a), which has not been observed. Conspicuous differences in these SERS spectra are also found in the bands at 1608, 1535, 1354, 988, and 920 cm^{-1}, respectively. The relative intensities of the 1608, 1535, and 1354 cm^{-1} bands (Figure 7) decrease much in passing to lower DHPZ sulfate concentration. On the basis of the surface selection rule, these vibrational modes should have a large Raman polarizability change in the *z* direction (with *z* lying to the local metal surface normal). Indeed, according to the DFT calculations and previous studies,[17,34−37] all these modes are mostly due to in-plane CH bending or ring stretching modes, as shown in Figure 8, with large components parallel to the metal surface, when the molecule tends to lie flat on the surface. On the other hand, the 988 and 920 cm^{-1} bands, which do not have components perpendicular to the metal surface when the planar portion of the molecule (Figure 8) has an end-on or at least significantly tilted orientation, exhibit intensity enhancement. Even though the SERS spectrum of DHPZ sulfate at the lowest concentration (Figure 7) is noisy in comparison with the other SERS spectra, the out-of plane skeletal and CH deformation modes could be observed with the same very weak relative intensity at 668 and 653 cm^{-1}.

As the concentration of adsorbate in the solution decreases, the occupancy of the adsorbed molecules on the surface must decrease. If our interpretation is correct, this could explain the changes observed in the SERS spectra at different concentrations. More specific, the effective molecular area of each

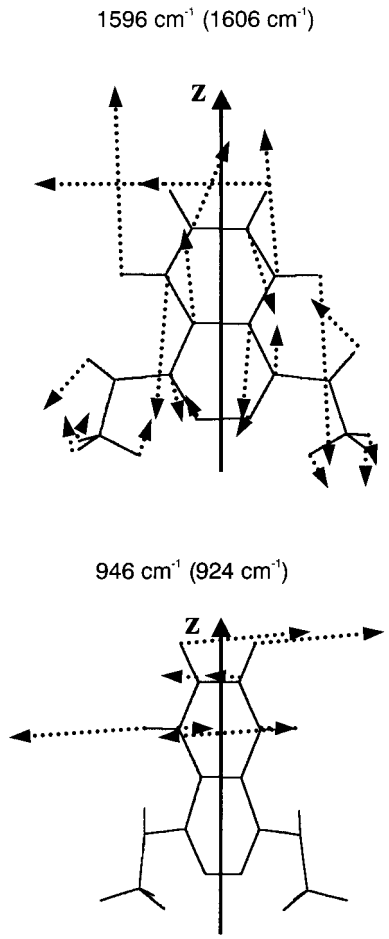

Figure 8. Fundamental calculated (BPW91/6-311+G(d)) vibrational modes of tautomeric form **1**, which implies out-of-plane CH bending modes and in-plane CH bending and ring stretching modes. Experimental SERS values are given in brackets.

adsorbed DHPZ sulfate on the Ag surface increases, that is, adsorbates prefer a less tilted orientation to the surface. Since an unequivocal SERS selection rule is not available, the exact tilt angle of the adsorbate cannot be estimated at the moment, however.

The SERS spectra of DHPZ sulfate (Figure 7a−c) present a medium broad band at around 230 cm^{-1}, which can be due to the Ag−N stretching mode, characteristic for the N-adsorbed species in SERS spectra under 250 cm^{-1}. This may indicate a bonding with the surface through the lone pairs of the nitrogens located on the phthalazine system. Unfortunately, this cannot be a decisive argument, even if the band is broad enough and stronger than the very weak one at 235 cm^{-1}, which has been ascribed to an out-of-plane skeletal deformation in the FT-Raman spectrum of DHPZ sulfate and may overlap in the SERS spectrum with the Ag−N stretching mode. According to the proposed orientation and the surface selection rule, the relative intensity of this skeletal distortion mode should increase, whereas the Ag−N stretching mode should decrease with a decrease in the DHPZ sulfate solution concentration.

With an increase in the DHPZ sulfate solution concentration, the SERS spectrum of DHPZ sulfate (Figure 7d,e) becomes very noisy, and up 10^{-4} mol L^{-1} no signal could be detected. This concentration may be sufficient to cause a coverage with DHPZ sulfate of the surface, and therefore, no SERS spectrum can be recorded upper this concentration. However, even if at about 10^{-5} mol L^{-1} the SERS spectrum (Figure 7d) is noisy and presents a significant background, totally symmetric modes of phthalazine (1452, 1382, 799, and 529 cm^{-1}) could be observed at almost the same position as in the SERS spectrum at 4.2×10^{-6} mol L^{-1} (Figure 7c), but with a smaller intensity. But other in-plane vibrational modes, as the in-plane CH stretching, ring stretching, CH deformation, and skeletal deformation modes, which have been assigned at almost the same wavenumbers, 1608, 1576, 1354, 1161, and 1116 cm^{-1}, respectively, as in the SERS spectrum at 4.2×10^{-6} mol L^{-1}, have higher or similar intensities. On the other hand, the 988 cm^{-1} band, for example, which has been ascribed to an out-of-plane CH deformation, exhibits intensity enhancement. One can notice that the 230 cm^{-1} band has also a similar broad profile, as at 4.2×10^{-6} mol L^{-1}, but perhaps a little enhanced. Taking into account all these spectral changes, we suppose that at this concentration (4.0×10^{-5} mol L^{-1}) the adsorbate has a rather random orientation to the Ag surface, as phthalazine in solution. As one increases the concentration, the SERS signal becomes weaker due probably to the surface coverage with DHPZ sulfate.

In conclusion, the computed structural parameters for tautomer **2** agree very well with the reported experimental data, while for tautomer **1** no crystal structure data were yet published. The theoretical calculations and the SERS spectra suggest that there is no surface photodecomposition of 1,4-dihydrazinophthalazine sulfate on the metal surface. SERS spectra of 1,4-dihydrazinophthalazine sulfate could be recorded even at nanomolar concentration with a conventional SERS setup. At about 10^{-6} mol L^{-1} the molecular skeletal plane is probably oriented perpendicular to, or at least significantly tilted with respect to, the Ag surface plane. As the concentration is decreased, the molecule tends to lie flat on the Ag surface. With the increase in solution concentration, a surface coverage with 1,4-dihydrazinophthalazine sulfate may occur.

Acknowledgment. We highly acknowledge the financial support from the Deutsche Forschungs gesellschaft (Sonderforschungsbereich SFB 347, Projekt C2) as well as from the Fonds der chemischen Industrie.

References and Notes

(1) Bein, H. J.; Brunner, H. *Ger. Offen.* **1972** (patent).
(2) Brunner, H.; Hedwall, Ph. R. *Ger. Offen.* **1973** (patent).
(3) Dorneanu, V.; Popovici, I.; Dorneanu, M. *Rom. Rev. Chim.* **1996**, *35*, 357.
(4) Micu-Semeniuc, R.; Semeniuc, R. F.; Cozar, O.; David, L. *Synth. React. Inorg. Met. −Org. Chem.* **1994,** *28*, 501.
(5) Thompson, L. K.; Woon, T. C. *Inorg. Chim. Acta* **1986**, *111*, 45.
(6) Tandon, S. S.; Thompson, L. K.; Hynes, R. C. *Inorg. Chem.* **1992**, *31*, 2210.
(7) Talwar, S. K.; Rastogi, V. K.; Saxena, R. C. *J. Indian Chem. Soc.* **1991**, *68*, 402.
(8) Kyota, J.; Ueno, N. *Jpn. Kokai Tokkyo Koho* **1997** (patent).
(9) Conte, G.; Lauro, S.; Ruol, A. *Clin. Ter.* **1966**, *39*, 441.
(10) Campus, S.; Rappelli, A.; Fabris, F.; Mathis, I. *Ital. Biol. Sper.* **1967**, *43*, 1847.
(11) Campus, S.; Fabris, F.; Rappelli, A.; Mathis, I. *Ital. Biol. Sper.* **1967**, *43*, 1851.
(12) Tasumi, M. *Kobunshi* **1974**, *23* (5), 362.
(13) Tasumi, M.; Takahashi, S. *Seibutsu Butsuri* **1973**, *13* (1), 319.
(14) Tasumi, M. *Kagaku no Ryoiki* **1980**, *34* (1), 14.
(15) Nie, S.; Emory, S. R. *Science* **1997**, *275*, 1102.
(16) Takahashi, M.; Fujita, M.; Ito, M. *Chem. Phys. Lett.* **1984**, 109, 122.
(17) Suh, J. S.; Jang, N. H.; Jeong, D. H.; Moskovits, M. *J. Phys. Chem.* **1996**, *100*, 805.
(18) Andzelm, J.; Wimmer, E. *J. Chem. Phys.* **1992**, *96*, 1280.
(19) Johnson, B. G.; Gill, P. M. W.; Pople, J. A. *J. Chem. Phys.* **1993**, *98*, 5612.
(20) Herrnstadt, C.; Mootz, D.; Wunderlich, H.; Möhrle, H. *J. Chem. Soc., Perkin Trans. 2* **1979**, *6*, 735.
(21) Stadnicka, K.; Lebioda, L. *Acta Crystallogr.* **1979**, *B35*, 770.

(22) Carugo, O.; Castellani, C. B.; Perotti, A. *Acta Crystallogr*. **1995**, *C51*, 1683.

(23) Lee, P.; Meisel, D. *J. Phys. Chem.* **1982**, *86*, 3391.

(24) Brandt, S. E. Cotton, T. M. *Physical Methods of Chem. Series*, 2nd ed.; Wiley: 1993; Vol. IXB, p 670.

(25) Frisch, M. J.; Trucks, G. W.; Schlegel, H. B.; Gill, P. M. W.; Johnson, B. G.; Robb, M. A.; Cheeseman, J. R.; Keith, T.; Petersson, G. A.; Montgomery, J. A.; Rhaghavachari, K.; Al-Laham, M. A.; Zakrzewski, V. G.; Ortiz, J. V.; Foresman, J. B.; Ciolowski, J.; Stefanov, B. B.; Nanayakkara, A.; Challacombe, M.; Peng, C. Y.; Ayala, P. Y.; Chen, W.; Wong, M. W.; Andres, J. L.; Replogle, E. S.; Gomberts, R.; Martin, R. L.; Fox, D. J.; Binkley, J. S.; Defrees, D. J.; Baker, J.; Stewart, J. P.; Head-Gordon, M.; Gonzalez, C.; Pople, J. A. *Gaussian 98*, Revision A7, Gaussian Inc.: Pittsburgh PA, 1998.

(26) Becke, A. D. *Phys. Rev.* **1988**, *A38*, 3098.

(27) Perdew, J. P.; Wang, Y. *Phys. Rev.* **1992**, *B45*, 13244.

(28) Becke, A. D. *J. Chem. Phys.* **1992**, *97*, 9173.

(29) Becke, A. D. *J. Chem. Phys.* **1993**, *98*, 5648.

(30) Lee, C.; Yang, W.; Parr, R. G. *Phys. Rev.* **1988**, *B37*, 785.

(31) Yamguchi, Y.; Frisch, M.; Gaw, J. F.; Schaefer, H. F.; Binkley, S. *J. Chem. Phys.* **1986**, *84*, 2262.

(32) Cremer, D.; Pople, J. A. *J. Am. Chem. Soc.* **1975**, *97*, 1354.

(33) Zefirov, N. S.; Palyulin, V. A.; Dashevskaya, E. E. *J. Phys. Org. Chem.* **1990**, *3*, 147.

(34) Mitchell, R. W.; Glass, R. W.; Merritt, J. A. *J. Mol. Spectrosc.* **1970**, *36*, 310.

(35) Muniz-Miranda, M.; Sbrana, G. *J. Raman Spectrosc.* **1996**, *27*, 105.

(36) McClellan, A. L.; Pimentel, G. C. *J. Chem. Phys.* **1955**, *23*, 245.

(37) Lippincott, E. R.; O'Reilly, E. J. *J. Chem. Phys.* **1955**, *23*, 238.

(38) Hehre, W. J.; Random, L.; Schleyer, P.v. R.; Pople, J. A. *Ab Initio Molecular Orbital Theory*; J. Wiley: New York, 1986.

(39) Scott, A. P.; Radom, L. *J. Phys. Chem.* **1996**, *100*, 16502.

(40) Wong, M. W. *Chem. Phys. Lett.* **1996**, *256*, 391.

(41) Fleischer, R.; Walfort, B.; Gburek, A.; Scholz, P.; Kiefer, W. Stalke, D. *Chem. Eur. J.* **1998**, *4*, 2266.

(42) Billmann, J.; Kovacs, J.; Otto, A. *Surf. Sci.* **1980**, *92*, 153.

(43) Otto, A. *Light Scattering in Solids*, Cardona M.; Guntherodt G., Ed.; Springer: Berlin, 1984; Vol. 4.

(44) Moskovits, M.; Suh, J. S. *J. Am. Chem. Soc.* **1985**, *107*, 6826.

(45) Jeong, D. H., Jang, N. H.; Suh, J. S.; Moskovits, M. *J. Phys. Chem B* **2000**, *104*, 3594.

(46) Varsany, G. *Assignments for Vibrational Spectra of Seven Hundred Benzene Derivatives*; J. Wiley & Sons: New York, 1974.

(47) Moskovits, M. *J. Chem. Phys.* **1982**, *77*, 4408.

(48) Moskovits, M.; Suh, J. S. *J. Phys. Chem.* **1988**, *92*, 6327.